HYDROLOGICAL PROCESSES
Hydrol. Process. 21, 1026–1044 (2007)
Published online 21 February 2007 in Wiley InterScience
(www.interscience.wiley.com) DOI: 10.1002/hyp.6277

Comparison of the performance of flow-routing algorithms used in GIS-based hydrologic analysis

John P. Wilson*, Christine S. Lam and Yongxin Deng
Department of Geography, University of Southern California, USA

Abstract:

Flow direction and specific catchment area were calculated for different flow-routing algorithms using TAPES-G and TauDEM. A fuzzy classification was used along with eight topo–climatic attributes to delineate six landscape classes from a 10-m USGS DEM. A series of maps and tabular outputs were produced to compare flow-routing predictions in different parts of the study area in the Santa Monica Mountains of southern California. The matched pair *t*-test was used to compare the performance of pairs of specific catchment area grids across six user-defined fuzzy landscape classes. The results show that (1) the 'source' cells predicted with the Dœ, DEMON, and FD8 algorithms were confined to hilltops; (2) two single flow-routing algorithms (Rho8, D8) produced poor results; and (3) the choice of flow-routing algorithm has potentially important consequences for the calculation of upslope contributing areas, sediment transport capacity, topographic wetness, and several other topographic indices. Copyright © 2007 John Wiley & Sons, Ltd.

KEY WORDS digital elevation models; flow-routing algorithms; GIS; terrain analysis

Received 22 March 2004; Accepted 19 December 2005

INTRODUCTION

The shape of the earth's surface plays a fundamental role in the hydrologic, geomorphic, and ecological processes operating at the earth's surface because it influences the movement of water, sediment, and other constituents within a landscape. As a consequence, terrain shape is also fundamental to the prediction of various surface and subsurface flow characteristics such as soil moisture and stream flow depth and velocity (Moore *et al.*, 1988, 1991; Sulebak *et al.*, 2000). Most of the patterns and processes that create and shape these characteristics operate at the meso- and topo-scales, and many of the solutions to environmental problems, such as accelerated soil erosion and nonpoint source pollution, require management strategies that are implemented at these scales as well (Moore and Hutchinson, 1991).

Many primary and secondary topographic attributes have been computed from square-grid, triangulated irregular and contour-based elevation networks, and incorporated in numerous environmental classification schemes and modeling frameworks during the past two decades (e.g. Dikau, 1989; Band *et al.*, 2000; Burrough *et al.*, 2001). The provision of gridded elevation data sets by many national mapping agencies coupled with the development and wide distribution of methods for converting spot height and contour elevation data to square grids (see Hutchinson (1989) for one such method) has contributed to the tremendous growth in the popularity of gridded elevation data sets and grid-based algorithms for calculating topographic attributes.

Three of the most popular attributes used in hydrologic models—specific catchment area (SCA), topographic wetness index, and sediment transport capacity index—rely on some form of flow-routing algorithm to calculate the upslope contributing area and transfer flow (water, sediment, nutrients) to lower adjacent points or areas in a landscape (Desmet and Govers, 1996; Mitasova and Mitas, 2002). Grid-based flow-routing algorithms allocate the outflow from a given cell to one or more downslope cells. There are two basic terrain features that may be responsible for directing flow from one digital elevation model (DEM) pixel to multiple downslope neighbors. The first is the presence of submeter terrain features that direct flow to neighboring cells other than the cell marking the path of maximum descent and the second is the presence of two or more neighboring cells that are lower in elevation. Few, if any, DEM-based flow-routing algorithms can resolve submeter features, but several can direct flow to two or more downslope cells (Endreny and Woods, 2003). Several studies have compared the performance of two or more flow-routing algorithms using a variety of criteria but they generally stop short of describing their coincidence with observed runoff behavior and/or their impact on runoff prediction (Peters *et al.*, 1995).

Wolock and McCabe (1995) compared topographic wetness index distributions computed with single and multiple flow-routing algorithms using topographic maps and surveys spread across ten states. The single flow-routing algorithm was similar to D8 (O'Callaghan and Mark, 1984) and the multiple-flow direction algorithm

* Correspondence to: John P. Wilson, Department of Geography, University of Southern California, Los Angeles, CA 90089-0255, USA. E-mail: jpwilson@usc.edu

incorporated similar concepts to FD8 (Quinn *et al.*, 1991). The mean wetness values estimated with the multiple-flow direction algorithm were higher and the magnitude of the topographic wetness index differences tended to increase as DEM resolution decreased. The multiple-flow direction algorithm also produced smoother patterns of topographic wetness index across the DEMs (indicating less abrupt variations in the magnitude of topographic wetness for adjacent cells). The impact of the topographic wetness index distributions calculated with the single- and multiple-flow direction algorithms on TOPMODEL (Beven and Kirkby, 1979) model efficiency and simulated flow paths were negligible when the model was calibrated by adjusting the subsurface hydraulic parameters.

Desmet and Govers (1996) compared the upslope contributing areas calculated with six different flow-routing algorithms for a small catchment in Flanders, Belgium. The D8 algorithm, 2-D aspect direction algorithm of Lea (1992), multiple-flow direction algorithms of Freeman (1991) and Quinn *et al.* (1991), ANSWERS routing algorithm (Beasley *et al.*, 1980), and their own flux decomposition flow-routing algorithm were coded in a series of IDRISI (Eastman, 1992) scripts. The multiple-flow direction algorithms produced distinctive spatial and statistical patterns depending on the maximum number of downslope cells to which flow could be directed. The two single flow-routing algorithms produced patterns of SCA different from each other and each of the multiple-flow direction algorithms. The multiple-flow direction algorithms produced much smoother distributions of SCA. Overall, Desmet and Govers (1996) favored the two algorithms that allowed flow to only one or two downslope neighbors because they (visually) produced stronger correlations with the main drainage lines. The main structure of the catchment (i.e. the interfluves and main drainage lines) was identified by all six-flow direction algorithms, and most of the variability occurred in higher elevation areas (based on the maps reproduced in the manuscript).

Desmet and Govers (1996) also examined the effect of the choice of the flow-routing algorithm on the predicted locations of ephemeral gullies. The multiple-flow direction algorithms were able to identify areas where ephemeral gully erosion is likely, but they could not predict the precise location of the gullies (which never exceeded half the width of the grid cells for this particular study area). The single flow-routing algorithms predicted ephemeral gullies to start higher on the slopes but the correspondence with observed patterns was erratic because these algorithms were very sensitive to small elevation errors.

Tarboton (1997) proposed the D∞ algorithm and compared its performance with D8, 2-D Lea, FD8, and Digital Elevation Model Network (DEMON) (Costa-Cabral and Burges, 1994) for several hypothetical surfaces and a pair of research catchments in Arizona and California. He believed that the best flow-routing algorithms would (1) avoid or minimize dispersion, (2) avoid or minimize grid bias, (3) increase the precision with which flow directions are resolved, (4) require a simple and efficient grid-based matrix storage structure, and (5) have the ability to cope with difficult data (saddles, pits, flat areas).

Tarboton (1997) found that D8, FD8, and D∞ generated different distributions of SCA in the two research watersheds. He argued that the D∞ predictions were superior because D8 resolves flow directions too coarsely (point 3 above) and therefore introduces grid bias (point 2), whereas FD8 introduces substantial dispersion (point 1), resulting in inefficient data storage. The D∞ method, based on triangular facets, also avoided the loops and other inconsistencies caused by the influence of higher neighbors and downslope flow that characterize the plane (fitting) flow methods of Lea (1992) and Costa-Cabral and Burges (1994). Finally, Tarboton (1997) criticized the randomness embedded in Rho8 (Fairfield and Leymarie, 1991), arguing that upslope and SCAs are deterministic quantities that should be computed in a repeatable way.

Wilson *et al.* (2000) examined the effect of the DEM source, grid resolution, and choice of flow-routing algorithm on five topographic attributes in a large forested catchment in southwest Montana. The SCA and sediment transport capacity index (Moore and Wilson, 1992, 1994) were computed with D8, Rho8, FRho8, and DEMON in terrain analysis program for the environmental sciences-grid (TAPES-G) (Gallant and Wilson, 1996, 2000) and assigned to five classes to facilitate the comparison of pairs of maps. The comparisons showed that (1) the single-flow-direction algorithms initiated flow from 30–40% of the cells and produced much higher proportions of cells with small upslope contributing areas and (2) the parallel flow paths generated with D8 take longer distances from the tops of slopes to accumulate large values of the upslope contributing area and SCA. The choice of cross-grading area threshold (which is utilized in TAPES-G to switch from FD8 to D8 and FRho8 to Rho8) produced very small (<5%) differences in both attributes. Overall, the results showed that FRho8 and DEMON agreed with each other in 71% of the grid cells and that the other pairs (D8-Rho8, D8-FRho8, D8-DEMON, etc.) agreed with each other in 49–57% of the grid cells.

Fried *et al.* (2000) calculated several topographic attributes and examined their potential for mapping stormwater contributing areas in Barnard Drain near Michigan State University's East Lansing campus. Static topographic wetness and sediment transport capacity indices were calculated with D8 and DEMON in TAPES-G and quasi-dynamic topographic wetness indices were calculated with dynamic wetness index-grid (DYNWET-G) (Barling *et al.*, 1994) and several sets of soil parameters. The quasi-dynamic wetness index incorporated both the topography in the upslope contributing area and time required for subsurface drainage to redistribute soil water. The calculated wetness and stream power indices were compared with independently identified flow paths (marked on topographic maps by two experts from the hydrologic unit of the Michigan Department of Environmental Quality) and GPS-referenced

DOI: 10.1002/hyp

field observations of wet areas. Examination of modeled flow paths overlaid on topographic contours showed that DEMON produced strands of high topographic wetness that were far more plausible than those produced with D8. The level of agreement between flow paths and strands of high dynamic topographic wetness was more difficult to assess, in part because the dynamic strands tended to be less well defined. The comparisons with field observations suggested more agreement than differences among the various models. While the D8 static model generated the highest level of agreement between the wet spots and high values of topographic wetness and/or sediment transport capacity indices, the variable soil dynamic model was a close second, and was preferred over the others for reasons related to model assumptions and its ability to predict the investigative buffer footprints more accurately. The areas of greatest disagreement occurred in relatively flat areas, lending credence to the conventional wisdom that flow path determination by any method is especially challenging in areas of low relief.

Endreny and Woods (2003) calculated a series of topographic attributes for two small fields in New Jersey and compared the spatial congruence of overland flow paths observed in the field to those predicted with D8, FD8, 2D-Lea, 2D-Jensen (Jensen, 1996), and D∞. The observed flow paths were field-sketched and then mapped on the DEM pixels for comparison with the computed flow paths. The lowest congruence ratings were produced with D8 (which constrained flow to a single neighbor) and FD8 (which directed flow into all neighbors that were lower in elevation). The 2-D Lea and D∞ algorithms, which direct flow to a maximum of two neighbors, produced the highest congruence ratings. Modified versions of D8 (using a buffer to direct flow to neighboring cells that overlapped the buffered area) and FD8 (limiting flow to 3 or 5 downslope neighbors) produced congruence rankings that rivaled those of the more sophisticated 2D-Lea and D∞ algorithms.

The results from these six studies show how different flow-routing algorithms behave differently over a small range of often-generalized landscapes (e.g. hypothetical circular cones, simplified hillslopes). However, it is difficult to compare a circular cone, for example, with the complicated terrain structures and features that characterize fluvial landscapes with moderate relief such as the Santa Monica Mountains of southern California. These landscapes can be flat, hilly and/or steep, and more work is needed to understand the consequences of choosing one of these algorithms over the others in these types of landscapes. Each flow-routing algorithm offers a unique method to calculate flow direction and upslope contributing area and they are likely to produce different terrain attributes in different landscapes and sometimes different parts of the same landscapes. This paper sought to advance our knowledge of these tradeoffs by testing two null hypotheses as follows:

Hypothesis 1: The performance of the D8, Rho8, D∞, DEMON, and FD8 flow-routing algorithms does not change as flow descends from steeper to flatter terrain.

Hypothesis 2: The performance of the same five algorithms does not vary across different landscape classes or units calculated with the fuzzy *k*-means algorithm of Burrough and McDonnell (1998).

STUDY AREA

The USGS 1:24K Point Dume, CA map quadrangle in the Santa Monica Mountains of southern California was used to compare flow-routing algorithm performance (Figure 1). This mountain range stretches 74 km from Point Mugu in Ventura County to Griffith Park in Los Angeles County in a narrow band that never exceeds 12 km in width. The mean elevation is 305 m and extends from 0 m at the coast to 948 m. The mountains are approximately five million years old with rugged terrain, relatively short flow paths, and rocky or gravelly soils (Huffman, 1998). The study area chosen for this project is located in the middle of the mountain range on the south side of the central ridgeline.

HYPOTHESIS TESTING

The following five-step procedure was utilized to test the two hypotheses. First, the 10-m USGS DEM for the study area was downloaded and clipped to eliminate some edge and ocean cells. Second, flow direction and SCA were calculated with five different flow-routing algorithms. Third, these results were compared, paying particular

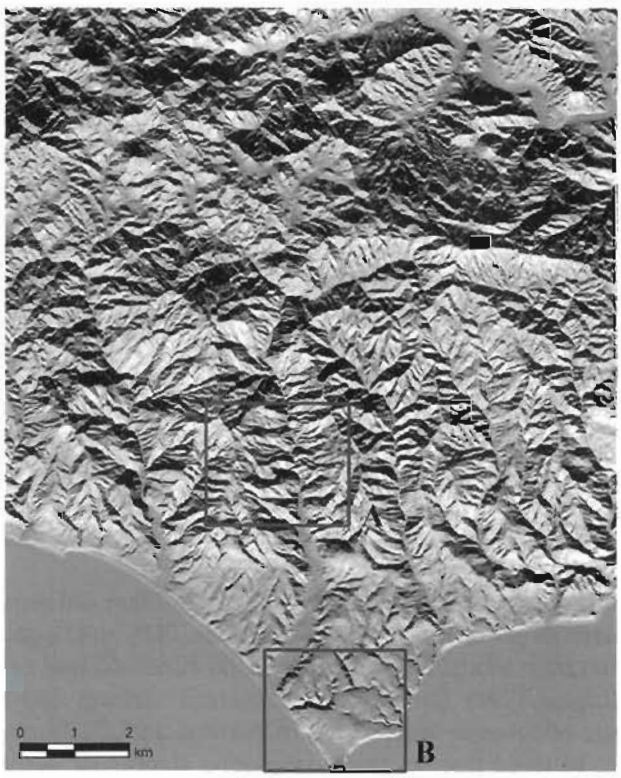

Figure 1. Map showing gray-scale Point Dume DEM plus two inset boxes labeled A and B

attention to differences in spatial pattern and magnitude of differences in the SCA. Fourth, eight primary and secondary topographic attributes were generated and used to classify the study area into a series of fuzzy landscape classes—the k-means fuzzy classification method is attractive because it is reproducible and generates mappable landform classes that correspond to field-observable landform structures. Finally, the computed SCA was tabulated by flow-routing algorithm and landscape class to identify those parts of the landscape where different flow-routing algorithms produced significantly different estimates of the SCA.

Data acquisition and preprocessing

The 10-m Point Dume, CA DEM (code 34 118a7) was downloaded from the web (http://data.geocomm.com). The projection was changed to NAD83 and UTM zone 11 using the nearest neighbor (default) option, and the initial quadrangle was clipped to a rectangle with 1118 rows and 1358 columns. The ocean cells were then masked out and their values reported as NODATA. The final DEM contained 1, 263, 296 cells.

Flow direction and specific catchment area calculations

Flow directions and SCAs were calculated with D8, Rho8, FD8, DEMON, and D∞ in TAPES-G and TauDEM that were downloaded free-of-charge from the web (see http://uscgislab.net and http://moose.cee.usu.edu/taudem/taudem.html for additional details). Spurious pits were not removed prior to running TAPES-G and TauDEM. Further details about the concepts and quirks incorporated in each of the flow-routing algorithms are provided below.

The D8 (deterministic eight-node) single-flow-direction algorithm directs flow from each grid cell to one of eight nearest neighbors based on the slope gradient (O'Callaghan and Mark, 1984). The aspect Ψ (measured in degrees clockwise from north) marks the direction of the steepest descent for each grid cell or point in a catchment and is the direction in which water would flow from that grid cell or point. Most implementations of D8 utilize the primary flow direction (FLOWD) for water moving over the land surface as an approximate replacement for aspect (Moore, 1996). The simplest method of calculating FLOWD is to determine the slope (S_i) to each neighbor:

$$S_i = \varphi(i)(z_9 - z_i)/\lambda \qquad (1)$$

where $\varphi(i) = 1$ for the NSEW neighbors, $\varphi(i) = 1/\sqrt{2}$ for the NE, SE, SW, and NW neighbors, z_9 refers to the elevation of the center grid cell, z_i is the elevation recorded for the eight neighboring grid points in a 3×3 moving window ($z_1, z_2, \ldots z_9$), and λ is the grid spacing (Gallant and Wilson, 2000). FLOWD was then set to 2^{J-1} where J is the direction for which S_i is highest. The upslope contributing area is the number of pixels whose flow reaches the pixel of interest multiplied by the pixel area, and the SCA is the upslope contributing area divided by the contour width, which is assumed to equal the 'width' of a grid cell. Some implementations of D8 utilize the grid spacing for both cardinal and diagonal flow assignments, while others, such as TAPES-G, assume that the grid cell width is a good estimate for flow width in the cardinal directions and that the cell width multiplied by $\sqrt{2}$ is the best estimate of the flow width for flow assignments to diagonal cells. There is little theoretical or empirical evidence to support one or the other of these options, and further research to clarify what types of estimates would work best in different circumstances is needed (Gallant *et al.*, 2000). The procedure coded in TAPES-G was utilized in this particular study.

The Rho8 (random eight-node) algorithm developed by Fairfield and Leymarie (1991) introduced a degree of randomness to break up the parallel flow paths that D8 tends to produce on planar surfaces (Wilson and Gallant, 2000). This algorithm starts by identifying all the downslope neighboring cells, then calculates the slope gradients in each of these directions, and finally extracts random numbers from a table to direct the flow to one of these candidate cells. The random numbers are allocated on a slope-weighted basis such that the potential flow paths with the steepest gradients have the greatest probability of being selected and the overall flow pattern more or less matches the one produced with D8. The upslope contributing and SCAs are calculated using the flow width and flow accumulation approaches adopted for D8, although a different flow network is produced each time the algorithm is used because of the random assignment of flow among multiple downslope cells (Wilson *et al.*, 2000).

The FD8 multiple-flow direction algorithm developed by Quinn *et al.* (1991) directs water to every adjacent downslope cell on a slope-weighted basis. Figure 2 shows how two weights—0·5 and 0·35 for cardinal and diagonal

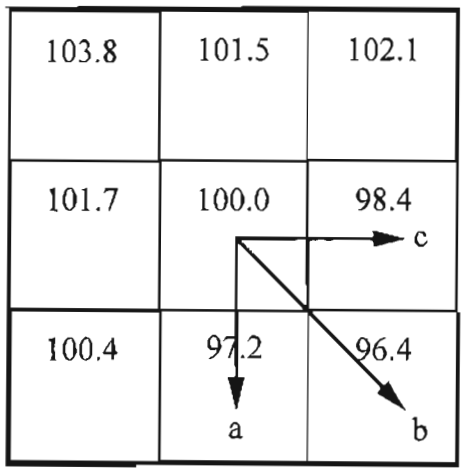

a = 0.50 * tan [(100.0 – 97.2) / dx1] = 0.002443 45.3%

b = 0.35 * tan [(100.0 – 96.4) / dx2] = 0.001555 28.8%

c = 0.50 * tan [(100.0 - 98.4) / dx1] = 0.001396 25.9%

Σ = 0.005394

Figure 2. Allocation of flow to multiple downslope cells using FD8 multiple-flow direction algorithm

DOI: 10.1002/hyp

directions respectively—plus slope gradients are utilized to calculate the proportion of flow assigned from the center cell to each downslope cell in a three-by-three moving window. The length *dx1* is set to 10 m (i.e. the cell spacing) and *dx2* to 14·14 m to mimic the flow path lengths in the cardinal and diagonal directions. Each cell receives only a fraction of the discharge from each upslope cell and, therefore, the upslope contributing area of the receiving cell is typically composed of partial contributions from many different cells. The SCA is calculated as the sum of the contributing areas from upslope cells divided by the cell width for cardinal flow directions and by the cell width multiplied by $\sqrt{2}$ for diagonal flow directions (similar to D8 and Rho8 in TAPES-G). A maximum cross-grading area threshold of 50 000 m^2 was also utilized with FD8 in this particular study to switch from multiple to single flow directions (i.e. D8), which means that flow dispersion was terminated whenever cells with upslope contributing areas $\geq$50 000 m^2 ($\geq$500 cells) were encountered.

The fourth algorithm called DEMON was developed by Costa-Cabral and Burges (1994) and determines the flow direction based on the local aspect angle, similar to Lea (1992). Both DEMON and 2-D Lea assume that flow moves across a planar surface in the direction of the steepest slope, or aspect angle, similar to a 'rolling ball' such that, if a ball was released from the center of a grid cell, it would travel down the steepest grade. This same rationale may be used to describe D8 but for the fact that Lea (1992) specified aspect in 1° increments (versus the 45° increments used for D8) and the flow generated over a pixel in DEMON is directed downslope over a two-dimensional flow strip (Costa-Cabral and Burges, 1994). These flow strips partition catchments into irregularly shaped elements that are defined by pairs of orthogonals and equipotential lines (contour lines). The width of the flow strips increases over divergent topography, decreases over convergent topography, and remains constant over planar surfaces (Figure 3(a)).

Figure 3(b) shows the sequence of flow paths in coordinate pairs that originated from the source pixel (1, 1) in Figure 3(a). Each branch corresponds to one stream tube in Figure 3(a). The amount of flow for each pixel is the flow accumulation of itself plus the amount of flow entering that pixel. When flow reaches an edge of a grid cell at a cardinal direction, then all flow is directed to the single neighbor. In other cases, the flow is split amongst the cardinal neighbors (Figure 3(c)). The fraction of flow distributed to each cardinal cell in Figure 3(c) is determined by

$$f_E = \frac{A_\Delta}{A} = \frac{1}{2}\frac{\Delta y}{\Delta x}\frac{1}{\tan(\alpha)} \tag{2}$$

$$f_S = 1 - f_E \tag{3}$$

where A_Δ is the dark triangular area where the flow is directed into the eastern neighbor, A is the pixel area $\Delta x \Delta y$ (where Δx or Δy refers to a pixel side), and α is the flow angle of the pixel. The upslope contributing

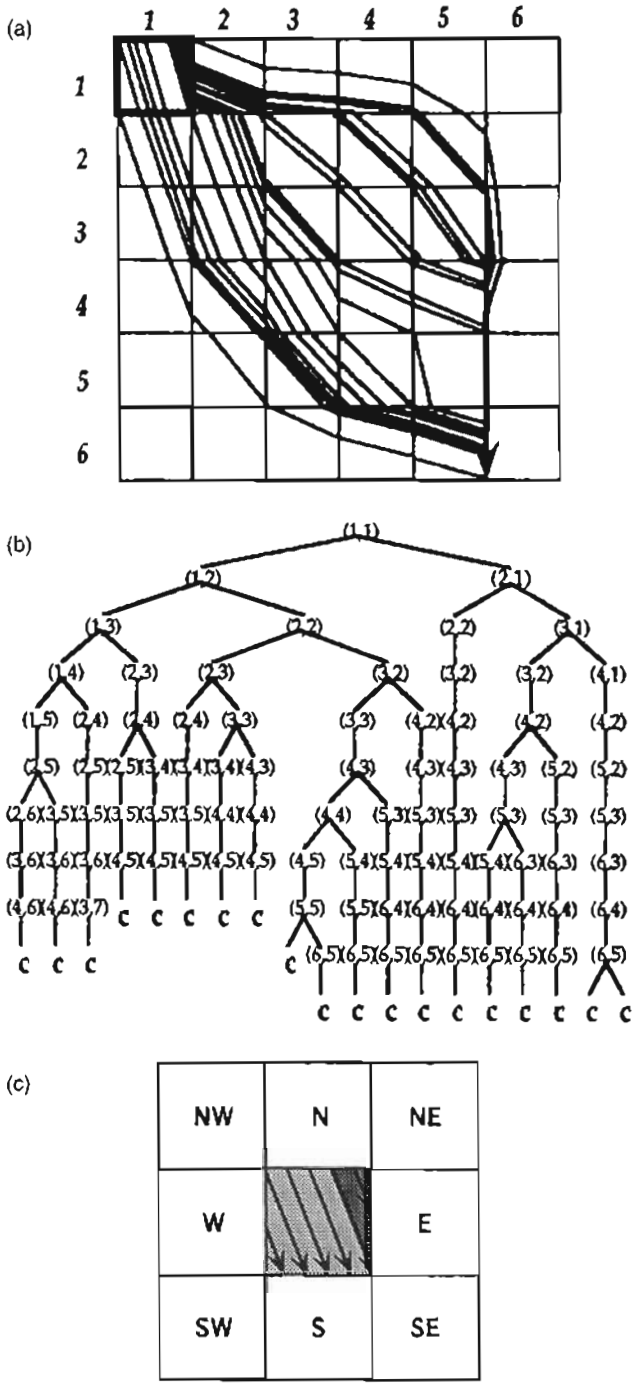

Figure 3. (a) Portion of grid showing flow tubes starting from pixel (1,1); (b) schematic representation of flow networks branching out in Figure 3(a); and (c) three-by-three moving cell window showing how flow from the source pixel is partitioned between two cardinal neighbors, E and S (from Costa-Cabral and Burges, 1994)

area for each cell in DEMON is computed by successive addition of the cell areas in each stream tube entering every pixel in the DEM, and the SCA is computed by dividing the upslope contributing area by the flow matrix width. The width (w) is determined using flow angles by

$$w = |\sin\alpha|\Delta x + |\cos\alpha|\Delta y \tag{4}$$

where Δx, Δy, and α are defined in Equation (2).

A modified version of DEMON is implemented in TAPES-G in which the nodes of the DEM define the

DOI: 10.1002/hyp

center of the pixels instead of the entire pixel area and the flow direction of a stream tube is defined by the aspect using

$$\Psi_{FD} = 180 - \arctan\left(\frac{z_y}{z_x}\right) + 90\left(\frac{z_x}{|z_x|}\right) \quad (5)$$

where z_x and z_y are vector components of the surface derivatives in the x and y directions (see Gallant and Wilson, 1996 for further details). The upslope contributing and SCAs are calculated in the same way as in the original version of DEMON (Costa-Cabral and Burges, 1994) in TAPES-G (Gallant and Wilson, 2000).

The final D∞ algorithm was proposed by Tarboton (1997) and incorporates several ideas from DEMON to assign multiple-flow directions to selected cells. The flow direction is determined in the direction of the steepest descent and is represented as a continuous angle between 0 and 2π radians. Figure 4 shows the calculation of flow directions using eight triangular facets in a 3 cell by 3 cell moving window. Each downslope vector is drawn outward from the center and may be at an angle that lies within or outside the 45° angle ($\pi/4$ radian) facet corner. If the slope vector angle falls within the facet, it represents the steepest flow direction of that facet; otherwise the steepest flow occurs along the steepest edge. Special rules are included to (1) force flat pixels to drain to a neighbor that ultimately drains to a lower elevation and (2) eliminate loops in the flow direction angles. Grid cells that are flat take flow direction from the D8 method in the original D∞ code, and the latest code uses the method of Garbrecht and Martz (1997) to assign flow directions to flat areas. The code returns NODATA for the flow direction for grid cells that are pits. The upslope area of each pixel is taken as its own area plus the fractional areas of upslope neighbors that drain into the pixel of interest, similar to FD8 and DEMON. If the angle falls on a cardinal or diagonal direction, then the flow from each cell drains to one neighbor. If the flow direction falls between the direct angle to two adjacent neighbors, the flow is proportioned between the two neighbor pixels according to how close the flow direction angle is to the direct angle for those pixels.

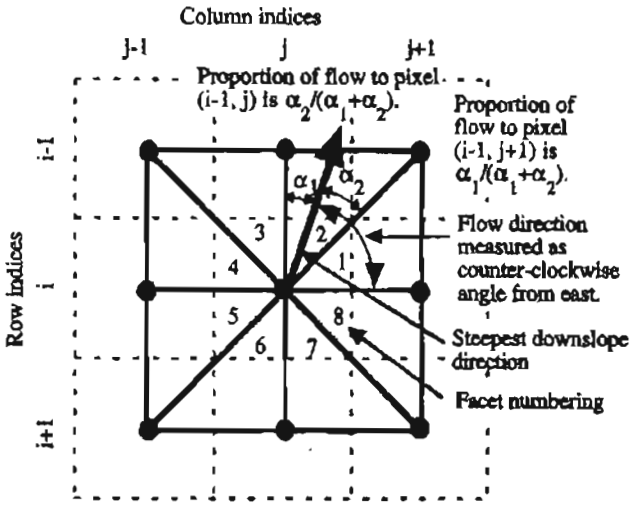

Figure 4. Flow direction on planar triangular facets in a block-centered grid (from Tarboton, 1997)

Fuzzy landscape classification

A series of landscape classes was identified using the fuzzy k-means classification method described by Burrough and McDonnell (1998). This method offers a quantitative, reproducible approach, which has been used in fields such as hydrology, soil science, and vegetation mapping. Burrough *et al.* (2001) calculated eight topographic attributes and used them with this method to divide a 10 000 km^2 portion of the Greater Yellowstone Area into six topo-climatic classes for example. The same topographic attributes—elevation, slope, plan and profile curvature, distance to ridgeline, topographic wetness index, solar radiation, and sediment transport capacity index—were used for the current study. The D8 algorithm was used to generate the topographic wetness and sediment transport capacity index values used here—the significance of this choice and the likelihood that it influenced the comparison of the flow-routing algorithm performance across the generated landscape classes is discussed in more detail later.

The FNX730 fuzzy k-means program that is supported by PCRaster (Karssenberg *et al.*, 2001) was applied to 690 randomly selected grid points. The procedure begins with a grouping of objects (cells) into a number of clusters, and then reassigns the objects among the clusters according to the similarity between these N objects and K cluster centers. The cluster center C of the cth cluster for the jth attribute x was calculated as the weighted average as follows:

$$C_{cj} = \sum_{i=1}^{N}(\mu_{ic})^q x_{ij} / \sum_{i=1}^{N}(\mu_{ic})^q \quad (6)$$

where the fuzzy exponent q (1·35) determined the amount of fuzziness or overlap. This iterative procedure continued until the algorithm found a stable solution in which objects were grouped into some prespecified number of clusters or classes. The membership μ of the ith object to the cth cluster was then determined by

$$\mu_{ic} = [(d_{ic})^2]^{-1/(q-1)} / \sum_{c'=1}^{K}[(d_{ic'})^2]^{-1/(q-1)} \quad (7)$$

where $d_{ic}{}^2$ is the square of the distance between the individual i and class center c according to the diagonal norm distance metric. The smaller the distance in attribute space, the greater the similarity of a data point to the class. This metric was computed using the following equation:

$$(d_{ic})^2 = \sum_{j=1}^{V}[(X_{ij} - C_{cj})/s_j]^2 \quad (8)$$

where s_j is the sample standard deviation for attribute j, V is the number of landscape classes, and X_{ij} and C_{cj} are as defined in Equation (6).

DOI: 10.1002/hyp

Two- to nine-class classifications were performed for this research, and the optimal number of classes (6) was then determined by using scaled partition coefficient F and classification entropy H, which express the overall fuzziness of the classification. The cluster (class) centers and ranges for the eight topographic attributes were then used to characterize the classes as ridgelines, steep north-facing slopes, steep south-facing slopes, stream channels, etc. Membership maps with values ranging from 0 to 1 were produced for each class to show the probability of each cell belonging to each class. High values indicate a high probability of membership in a particular class and vice versa.

Specific catchment area comparisons

The TAPES-G and TauDEM results were imported into ArcGIS 8·3 for grid analysis and map display. Two forms of statistical analyses were performed and two sets of inset maps were prepared to illustrate the performance of the five flow-routing algorithms in more detail.

The first set of statistical tests focused on 'low flow' and 'channel' cells since these grid cells have predictable hydrologic behaviors. Those grid cells with SCA $\leq$ 10 m^2 m^{-1} were categorized as 'low flow' cells because overland flow was not likely to occur in these parts of the landscape, and grid cells with SCA $\geq$ 5300 m^2 m^{-1} were characterized as cells crossed by stream channels. The 5300 m^2 m^{-1} threshold was obtained by summing the grid cells crossed by streams recorded in the USGS Point Dume Digital Line Graph (DLG) hydrography dataset and then selecting the same number of cells with large SCA values computed with D8. The purpose of isolating these cells was to determine whether the flow-routing algorithms predicted similar numbers and spatial patterns of 'low flow' and 'channel' cells since these cells mark the tops and bottoms of catchments. The grid cells with SCA $\geq$ 5300 m^2 m^{-1} predicted with each flow-routing algorithm were also compared to the 1 : 24K USGS DLG stream network to evaluate the overlap between this network and the computer-generated stream networks.

The second form of statistical analysis focused on the differences between pairs of SCA grids by landform class. Every one-thousandth cell was selected, with the

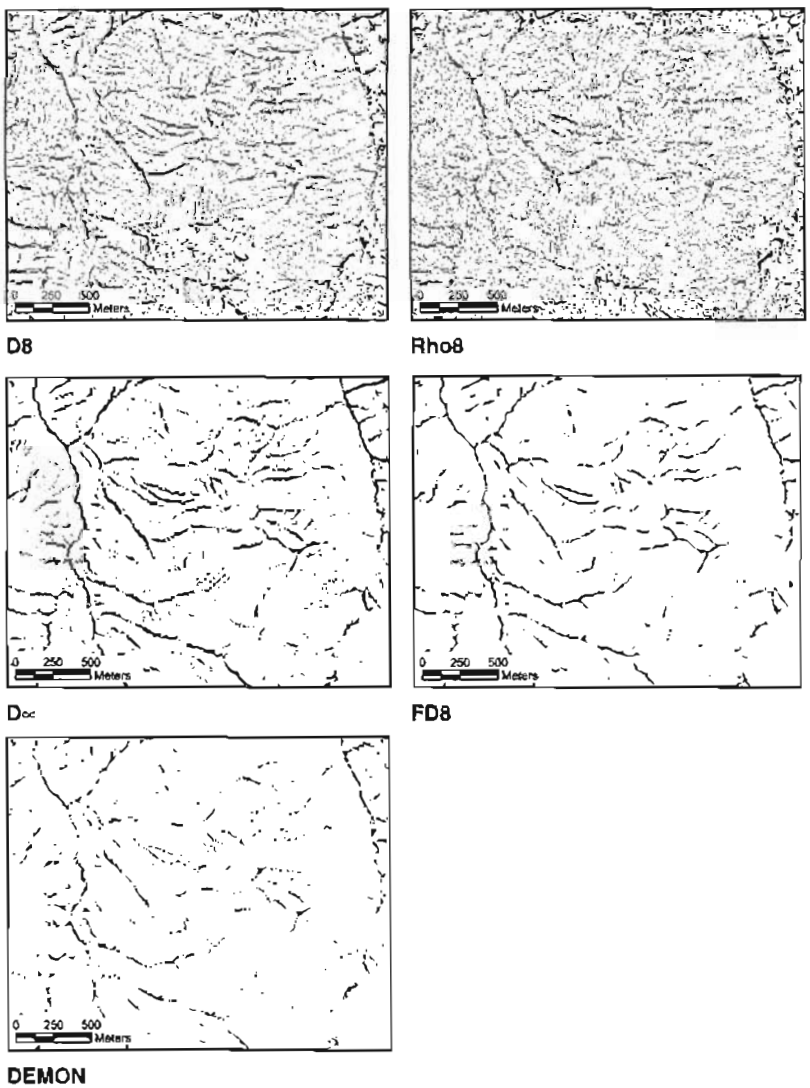

Figure 5. Series of maps showing SCA values <10 m^2 m^{-1} for each flow-routing algorithm in inset A in Figure 1

DOI: 10.1002/hyp

first cell location chosen randomly, and difference of means parametric matched pairs t-tests were performed to determine whether the differences between values in pairs of SCA grids were significantly different from zero.

RESULTS

Variations in specific catchment area in study area

Table Ia lists the basic SCA statistics by the flow-routing algorithm. The minimum values varied because different rules were used to direct the flow from each source cell to one or more adjacent downslope cells. The maximum values are similar because they represent watershed outlets at the coast. The mean values varied from a low of 3429 m^2 m^{-1} (DEMON) to a high of 4356 m^2 m^{-1} (FD8)—a difference of 27%. Table Ib partitions the SCA into a series of classes and indicates the percentage of cells for each flow-routing algorithm that fall into each class. These results show that D8 and Rho8, and to a lesser extent D∞, have many more 'low flow' cells (i.e. SCA $\leq$ 10 m^2 m^{-1}). The same pattern is repeated for the second class although the magnitude of the differences is reduced. The largest number of cells in classes 3 through 6 was generated with different flow-routing algorithms—D∞ for class 3, DEMON for class 4, and FD8 for the fifth and sixth classes—although the differences were relatively small.

The maps in Figure 5 show cells with SCA $\leq$ 10 m^2 m^{-1} for each flow-routing algorithm. The final three maps indicate that the patterns produced with DEMON, FD8, and to a lesser extent D∞, follow ridgelines. Rho8 and D8 produced more ubiquitous patterns in that some source cells followed the ridgelines, but others were scattered throughout the study area. At the other extreme are the cells that might be classified as part of the channel system. Figure 6 shows how the five algorithms predicted similar and more detailed channel systems than the 1 : 24K DLG for the same region. Over 80% of the same channel cells were predicted by each pair of flow-routing algorithms, whereas <50% of the cells were classified as channel cells with both the DLG and any one of the computer-based flow-routing algorithms.

Division of study area into fuzzy landscape classes

Figure 7 shows the eight topo-climatic attribute maps. The first map shows higher elevations along the east and west boundaries and, when viewed in conjunction with the slope map, shows the main channel moving from north to south with gentle slopes surrounding it. Footslopes are marked by cells with low (concave) profile curvatures in the third map as expected. A series of alternating north- (dark color) and south-facing (light color) slopes is clearly evident in the solar radiation map. The topographic wetness index and sediment transport capacity index maps show finer scale variability associated with water movement across this landscape.

Table II summarizes basic statistics for the eight topo-climatic attributes calculated at the 690 sample points using PCRaster, and shows a landscape with moderate relief (≈700 m), many steep slopes (22° mean), and large variations in terms of plan and profile curvature, solar radiation, topographic wetness, and sediment transport capacity index. Several variables have nonnormal distributions—distance to ridgelines (RDPRX) has a small number of very large values, annual solar radiation (SOLAR) has a small number of small values, and WET has a small number of large values for example. Table III shows correlation coefficients for each pair of variables

Table I. (a) Specific catchment area statistics for study area (units are in m^2 m^{-1}) and (b) % of cells per specific catchment area class

(a)

	Number of cells	Minimum	Maximum	Mean	Standard deviation
D8	1 263 296	7·07	2 237 670·25	3715·27	60 584·28
Rho8	1 263 296	7·07	2 236 030·25	3714·18	60 469·64
D∞	1 263 296	10·00	2 236 762·00	3934·18	61 469·07
FD8	1 263 296	2·56	2 341 777·00	4355·83	69 911·69
DEMON	1 263 296	7·07	2 214 353·00	3428·91	55 657·18

(b)

	SCA classes (m^2 m^{-1})						
	1 (≤ 10.0)	2 (10.1–20)	3 (20.1–40)	4 (40.1–70)	5 (70.1–100)	6 (100.1–1000)	7(>1000)
D8	12·8	18·5	26·9	16·3	7·2	13·3	5·1
Rho8	13·4	21·6	25·0	14·3	6·7	14·0	5·1
D∞	7·6	12·9	29·9	20·1	7·9	16·0	5·7
FD8	4·5	12·1	24·5	20·7	10·0	23·2	5·2
DEMON	2·7	12·2	29·3	23·6	9·6	17·6	5·0

DOI: 10.1002/hyp

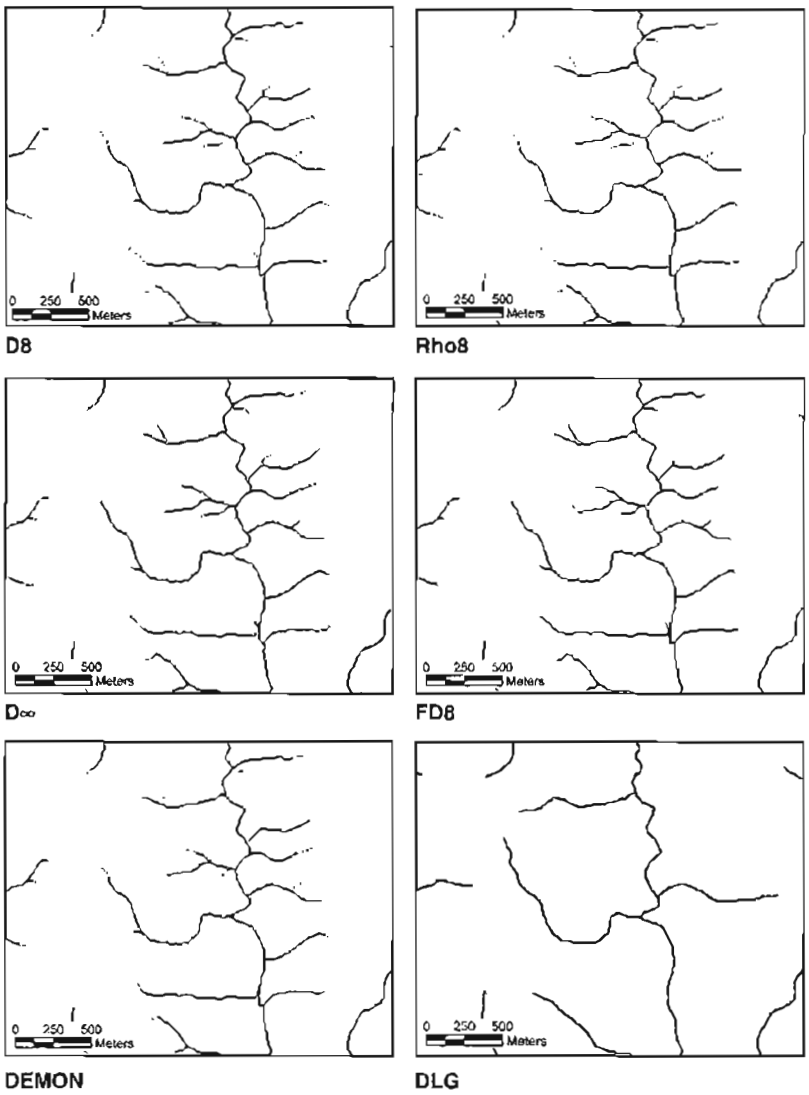

Figure 6. Series of maps showing SCA values ≥ 5300 m^2 m^{-1} for each flow-routing algorithm and 1:24K DLG in inset A in Figure 1

Table II. Basic statistics for sampled input data (N = 690)

Input data and units (where appropriate)	Mean	Standard deviation	Minimum	Maximum
ELEV (m)	364·84	189·41	2·00	764·50
SLOPE (degrees)	22·23	10·73	0·00	52·18
PROFC (m/m^2)	−0·17	1·93	−10·74	8·25
PLANC (m/m^2)	0·06	2·05	−7·48	13·15
RDPRX (m)	12·86	9·89	0·00	62·43
SOLAR ($*10^9 J/m^{2*}year$)	1024·60	206·09	369·50	1300·32
WET	7·28	1·96	4·51	18·56
SED	3·46	1·43	−12·78	9·32

Table III. Correlation coefficients for pairs of topo-climatic attributes (N = 690)

Attributes	ELEV	SLOPE	PLANC	PROFC	RDPRX	WET	SED	SOLAR
ELEV	—	—	—	—	—	—	—	—
SLOPE	0·31	—	—	—	—	—	—	—
PLANC	−0·04	0·00	—	—	—	—	—	—
PROFC	0·10	−0·01	−0·44	—	—	—	—	—
RDPRX	−0·06	0·15	0·43	−0·33	—	—	—	—
WET	−0·15	−0·42	0·57	−0·34	0·42	—	—	—
SED	0·11	0·51	0·53	−0·32	0·53	0·49	—	—
SOLAR	−0·02	−0·15	−0·11	0·10	−0·04	−0·04	−0·18	—

DOI: 10.1002/hyp

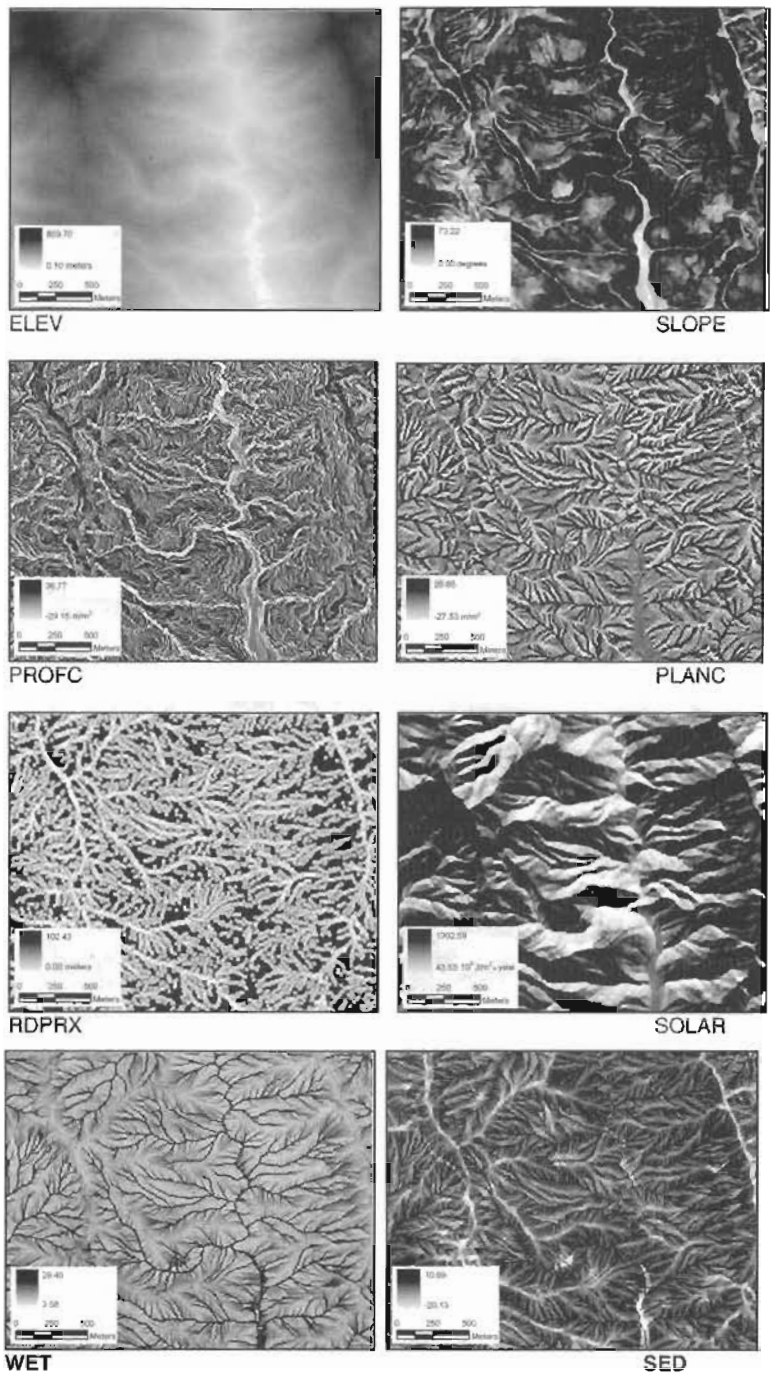

Figure 7. Maps showing the eight topo-climatic attributes in inset A in Figure 1 that were used in the fuzzy *k*-means classification. Gray scales range from low values (white color) to high values (dark colors)

at the 690 sample points. These results indicate relatively weak or nonexistent correlations for 24 of the 28 pairs of variables, such that these are not likely to cause problems in the subsequent analysis.

Table IV shows the mean topo-climatic attribute values for each of the six classes while Table V shows the ranges for the same variables. Although there were many overlapping values, this result was expected and the presence of overlapping values did not interfere with the identification and interpretation of the final landscape classes.

Figures 8 and 9 show the fuzzy *k*-means membership values calculated for each of the six landscape classes in insets A and B, respectively. These two areas were used along with the statistics summarized in Tables IV and V to help clarify the differences between the six classes as follows:

- Class 1 consists of coastal plains/gentle slopes because it has the lowest elevations, lowest slopes, and relatively high topographic wetness index. There is a small number of cells with high membership values for this class in inset A (Figure 8) in contrast to inset B (Figure 9) where 50% of the grid cells are highlighted in black and represent flat and gentle sloping areas along the coast.

DOI: 10.1002/hyp

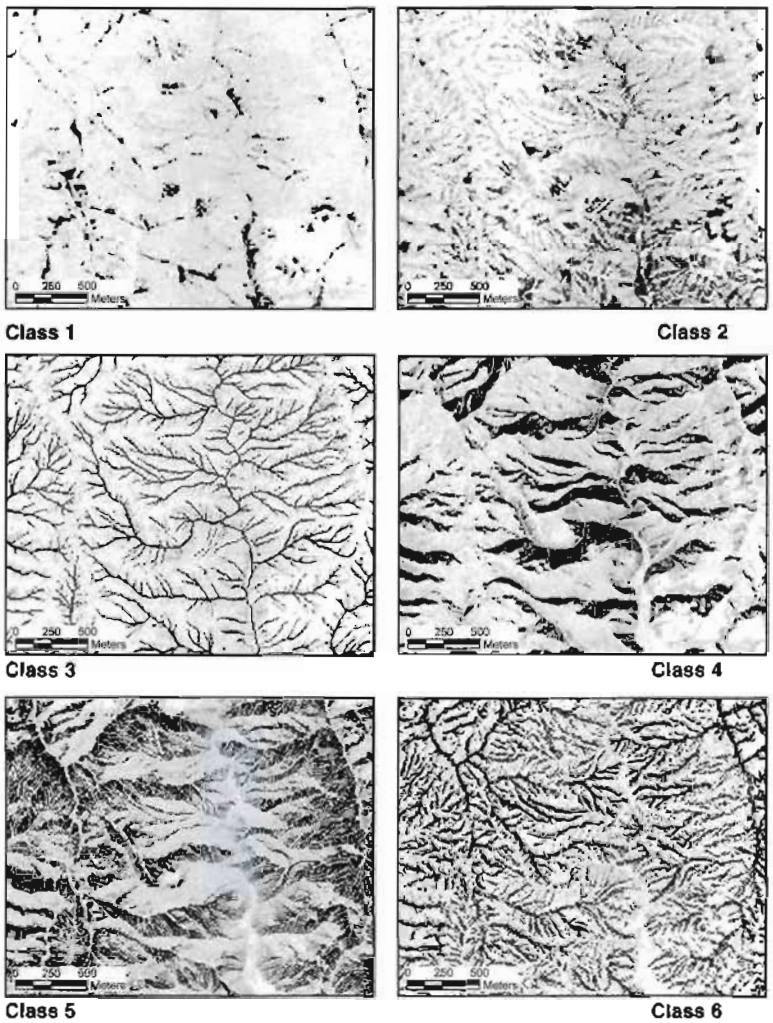

Figure 8. Maps showing the landscape class memberships in the inland area (inset A in Figure 1). Values range from 0 (low; white) to 1 (high; black)

Table IV. Cluster centers for six landscape classes

Input data	Class 1	Class 2	Class 3	Class 4	Class 5	Class 6
ELEV	178·14	195·34	382·77	440·40	444·55	454·06
SLOPE	7·47	16·56	20·59	29·72	26·90	24·85
PROFC	0·10	−0·46	−1·93	−0·59	−0·19	1·34
PLANC	−0·27	0·44	3·75	0·19	0·05	−2·08
RDPRX	7·17	22·38	19·24	15·15	13·84	2·03
WET	7·69	8·25	10·82	6·64	6·74	5·63
SED	1·50	3·60	5·53	3·96	3·80	2·93
SOLAR	1102·08	1082·83	972·13	720·18	1154·82	1064·24

- Class 2 consists of moderately steep lower valley slopes given the relatively low mean elevation, moderate slopes, and tendency for this class to occur immediately upslope of class 1 in Figures 8 and 9.
- Class 3 consists of stream channels because these grid cells had the highest mean sediment transport capacity index, lowest profile curvature, and largest planform curvature values (Table IV).
- Class 4 consists of steep north-facing slopes because the cells had the steepest slopes and lowest mean solar radiation index values.
- Class 5 consists of steep south-facing slopes because these cells recorded the largest mean solar radiation index and second steepest slopes. Figure 8 shows a series of alternating north- and south-facing hillslopes that represent classes 4 and 5.
- Class 6 consists of hilltops/ridgelines given the short distance to ridgelines and convex profile curvatures. The final map in Figure 8 shows the ridgelines as a series of linear features and therefore shows the watershed boundaries in this part of the Santa Monica Mountains.

Figure 10 shows the final crisp classification for insets A and B. These maps were produced by choosing the maximum membership value for each cell and assigning the cell to that class. The study area is divided into six distinctive landscape classes in both maps. The first map (inset A) shows ridgelines that run from west to east hugged by alternating bands of north- and south-facing slopes. The stream channels (class 3) are visible with gentle (class 1) and moderately steep (class 2) slopes flanking the valley bottoms. The second (inset B) map shows large numbers of class 1 cells, some class 2 cells, few channel (i.e. class 3) cells, and much smaller

DOI: 10.1002/hyp

Table V. Cluster ranges for six landscape classes

Input data	Class 1	Class 2	Class 3	Class 4	Class 5	Class 6
ELEV	0·1–859·7	0·3–723·6	0·3–836·5	6·7–852·1	7·1–858·5	6·4–859·7
SLOPE	0–27·6	0·1–56·7	0·1–66·8	7·9–73·2	4·4–61·1	1·2–70·3
PROFC	−7·8–11·1	−12·8–11·4	−29·1–8·3	−24·3–12·1	−16·4–14·2	−6·6–36·8
PLANC	−9·8–7·1	−4·7–6·4	−2·6–26·7	−9·0–13·0	−6·4–8·7	−27·5–6·1
RDPRX	0–80·7	0–84·9	0–66·6	0–76·6	0–54·1	0–34·14
WET	5·3–30·2	5·3–19·3	4·6–23·3	3·8–12·1	4·3–11·6	3·6–9·6
SED	0–80·1	0·1–1488·8	1·5–43 736·8	7·5–2336·5	4·5–1374·1	0·4–451·7
LAR	7·2–12·9	5·1–13·0	0·6–13·0	0·4–11·5	8·7–13·0	2·1–13·0

percentages of the other classes (as would be expected on the coastal plain). Overall, this method assigned 20% of the grid cells in the study area to the hilltop/ridgeline class and 44% of the cells to either the steep north- or south-facing slope classes. Smaller areas were classified as coastal plains/gentle slopes (14%), moderately steep lower valley slopes (13%), and stream channels (8%).

Variations in specific catchment area by crisp landscape class

Table VI shows that the lowest mean SCA values were associated with hilltops/ridgelines (class 1), the next lowest SCA values were associated with steep north- and south-facing slopes (classes 2 and 3), and then progressively larger mean SCA values were associated with moderately steep lower valley slopes (class 4), coastal plains/gentle slopes (class 5), and stream channels (class 6). The mean SCA values for streamlines are more than 1000 times larger than the equivalent values for hilltops/ridgelines for all five algorithms.

The mean SCA values generated for each landscape class with the five algorithms are ranked in descending order in Table VII. These ranks show how D8 started out with the lowest values in high elevation areas but passed DEMON and later Rho8 near or in the cells crossed by stream channels. FD8, in contrast, generated the highest SCA values everywhere except for the moderately steep lower valley slope class. Rho8 produced moderate SCA values except for the moderately steep lower valley slope class. Dᵒᵒ generated relatively

Table VI. Basic statistics for the six landscape classes

Hilltops/ridgelines

	Number of cells	Minimum	Maximum	Mean	Standard deviation
D8	256 012	7·07	1020·00	11·17	9·80
Rho8	256 012	7·07	20 010·00	19·79	96·88
Dᵒᵒ	256 012	10·00	221 819·59	25·32	649·54
FD8	256 012	2·61	2518·62	31·03	56·49
DEMON	256 012	7·07	5354·05	29·01	39·85

Steep north-facing slopes

	Number of cells	Minimum	Maximum	Mean	Standard deviation
D8	231 180	7·07	1 331 440.13	59·94	2772·17
Rho8	231 180	7·07	1 331 560.13	81·60	2913·36
Dᵒᵒ	231 180	10·00	1 324 101.75	92·23	3197·05
FD8	231 180	6·88	1 388 653.38	104·32	2896·00
DEMON	231 180	7·21	1 024 348.25	80·25	2136·99

Steep south-facing slopes

	Number of cells	Minimum	Maximum	Mean	Standard deviation
D8	323 989	7·07	189 568·25	50·71	344·06
Rho8	323 989	7·07	240 810·02	64·00	726·20
Dᵒᵒ	323 989	10·00	268 053·16	74·74	861·78
FD8	323 989	7·03	277 158·94	89·81	513·94
DEMON	323 989	7·35	236 130·02	66·52	426·78

Moderately steep lower valley slopes

	Number of cells	Minimum	Maximum	Mean	Standard deviation
D8	169 173	7·07	1 909 520·13	544·67	19 796·89
Rho8	169 173	7·07	2 142 250·25	799·06	23 476·90
Dᵒᵒ	169 173	10·00	1 827 493·00	790·89	18 204·57
FD8	169 173	4·65	1 989 181·38	656·07	22 591·25
DEMON	169 173	7·33	1 903 825·00	541·72	18 572·21

Coastal plains/gentle slopes

	Number of cells	Minimum	Maximum	Mean	Standard deviation
D8	177 787	7·07	2 215 020·25	2329·91	58 059·13
Rho8	177 787	7·07	2 213 440·25	2544·89	59 710·61
Dᵒᵒ	177 787	10·00	2 214 601·50	2718·39	57 533·74
FD8	177 787	2·56	2 315 620·50	2723·64	65 746·97
DEMON	177 787	7·07	2 123 134·50	2240·48	54 506·56

Stream channels

	Number of cells	Minimum	Maximum	Mean	Standard deviation
D8	103 888	7·07	2 237 670·25	39 942·29	191 625·53
Rho8	103 888	7·07	2 236 030·25	39 021·15	189 748·36
Dᵒᵒ	103 888	10·00	2 236 761·75	41 371·32	195 347·22
FD8	103 888	6·52	2 341 776·75	46 600·97	221 757·86
DEMON	103 888	7·45	2 214 353·25	36 517·30	175 534·55

Table VII. Mean SCA values ranked by flow-routing algorithm and landscape class

	Hilltops/ridgelines	North-facing slopes	South-facing slopes	Moderately steep lower valley slopes	Coastal plains/gentle slopes	Stream channels
D8	5	5	5	4	4	3
Rho8	4	3	4	1	3	4
D∞	3	2	2	2	2	2
FD8	1	1	1	3	1	1
DEMON	2	4	3	5	5	5
Magnitude	2·78	1·74	1·77	1·48	1·22	1·28

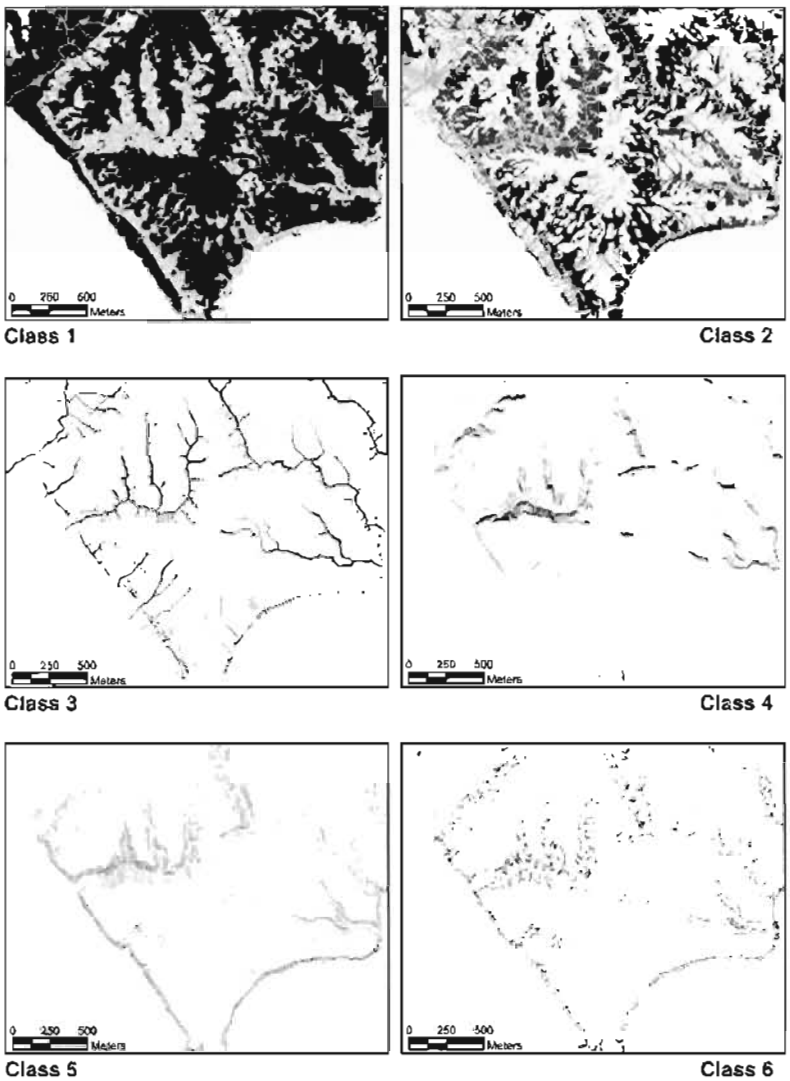

Figure 9. Maps showing the landscape class memberships along the coast (inset B in Figure 1). Values range from 0 (low; white) to 1 (high; black)

high SCA values in all but the hilltop/ridgeline class. DEMON generated relatively high SCA values along hilltops and ridgelines but produced the lowest mean SCA values on lower valley slopes, coastal plains, and in stream channels. The last row of Table VII shows the magnitude of differences in mean SCA values obtained by dividing the highest mean SCA value by the lowest mean SCA value in each landscape class and points to a reasonably consistent pattern in which the magnitude diminishes from the top of the landscape (i.e. cells classified as hilltops and ridgelines) to sea level (i.e. cells classified as stream channels and coastal plains/gentle slopes).

The difference of mean parametric matched pairs *t*-test results, summarized in Table VIII, show some important trends about the variability of SCA on different parts of the landscape. The *t*-test values marked with a show those instances when the null hypothesis can be rejected at the 1% level of significance and those marked with b indicate those instances when the null hypothesis can be rejected at the 5% level. The null hypothesis that the mean difference is not significantly different from zero

DOI: 10.1002/hyp

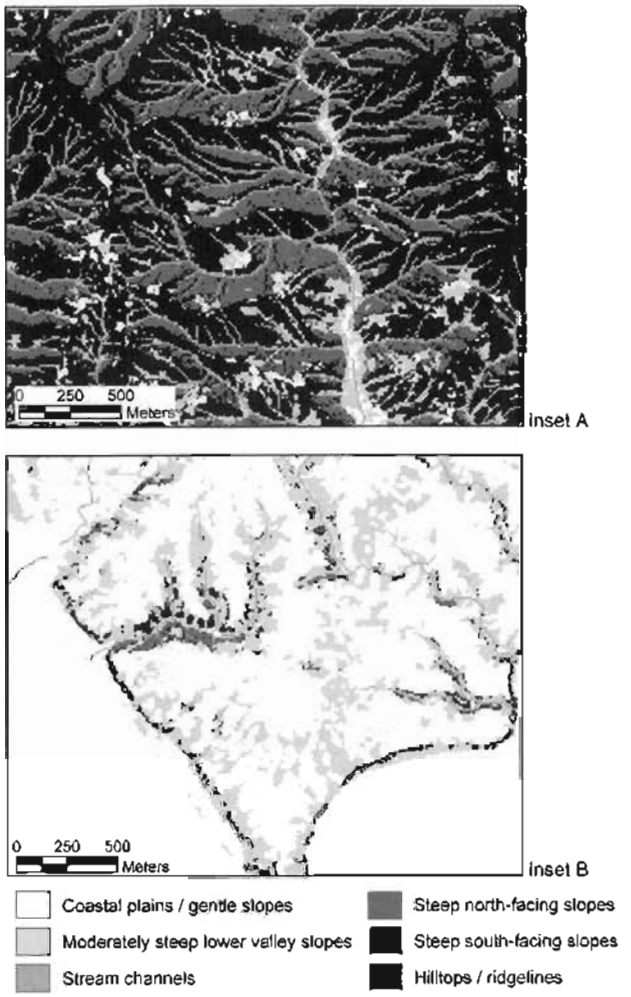

Figure 10. Maps showing the crisped landscape classes in insets A and B in Figure 1

Table VIII. Difference of means matched pairs parametric *t*-test results

Class 1—Coastal plains/gentle slopes

	D8	Rho8	Dꝏ	FD8	DEMON
D8	—	—	—	—	—
Rho8	−1·61	—	—	—	—
Dꝏ	0·98	0·99	—	—	—
FD8	−1·13	−1·05	−1·00	—	—
DEMON	−0·19	1·01	−0·98	1·01	—

Class 2—Moderately steep lower valley slopes

	D8	Rho8	Dꝏ	FD8	DEMON
D8	—	—	—	—	—
Rho8	1·78	—	—	—	—
Dꝏ	0·85	−1·96	—	—	—
FD8	−0·38	−2·26[b]	−1·16	—	—
DEMON	−0·55	−2·16[b]	−1·19	0·16	—

was rejected in 8 of 10 instances for hilltops/ridgelines but zero times for coastal plains/gentle slopes. Overall, the results summarized in Tables VII and VIII indicate

Class 3—Stream channels

	D8	Rho8	Dꝏ	FD8	DEMON
D8	—	—	—	—	—
Rho8	1.02	—	—	—	—
Dꝏ	−0.94	−1.15	—	—	—
FD8	−1.82	−1.44	0.82	—	—
DEMON	2.40[b]	0.08	1.17	2·71[a]	—

Class 4—North-facing slopes

	D8	Rho8	Dꝏ	FD8	DEMON
D8	—	—	—	—	—
Rho8	−1·04	—	—	—	—
Dꝏ	−2·20[b]	−1·42	—	—	—
FD8	4·00[a]	−3·33[b]	−1·98[b]	—	—
DEMON	−3·78[a]	−1·09	0·76	3·08[a]	—

Class 5—South-facing slopes

	D8	Rho8	Dꝏ	FD8	DEMON
D8	—	—	—	—	—
Rho8	−0·94	—	—	—	—
Dꝏ	−2·24[b]	0·40	—	—	—
FD8	−5·12[a]	−0·45	−2·37[b]	—	—
DEMON	−3·46[a]	0·50	0·71	3·91[a]	—

Class 6—Hilltops/ridgelines

	D8	Rho8	Dꝏ	FD8	DEMON
D8	—	—	—	—	—
Rho8	−3·55[a]	—	—	—	—
Dꝏ	−10·97[a]	1·38	—	—	—
FD8	−5·94[a]	−3·67[a]	−3·44[a]	—	—
DEMON	−10·93[a]	−5·22[a]	−6·81[a]	1·16	—

[a] Null hypothesis rejected at 1% level of significance.
[b] Null hypothesis rejected at 5% level of significance.

that the landscape classes can be divided into two groups based on the SCA values calculated with the five flow-routing algorithms. The first group consists of the high elevation landscape classes—hilltops/ridgelines plus steep north- and south-facing slopes—for which the null hypothesis was rejected in ≥50% of the cases and the second group consists of the low elevation landscape classes—moderately steep lower valley slopes, stream channels, and coastal plains/gentle slopes—for which the null hypothesis was rejected in <20% of the cases.

The counts summarized in Table IX display the variability in the performance of the five flow-routing algorithms in these two groups of landscape classes in more detail. The SCA values estimated with Rho8 and Dꝏ were most like each other (the null hypothesis was never rejected) in the three high elevation landscape classes. D8 and Rho8, Rho8 and DEMON, and Dꝏ and DEMON started out differently (the null hypothesis was rejected

DOI: 10.1002/hyp

at the 5% level of significance for hilltops/ridgelines) but produced similar results on steep north- and south-facing slopes (Table VII). The SCA values estimated with D8 were never similar to those produced with Dᵢₒ, FD8, and DEMON (the null hypothesis was rejected for all three high elevation classes) and similar results were obtained for FD8—the counts in Table IXa show that the null hypothesis was rejected in all three cases for D8 and Dᵢₒ, and in two of three cases for Rho8 and DEMON.

Table IX. Number of times null hypothesis was rejected for three groups of landscape classes

(a) High elevation landscape classes

	D8	Rho8	Dᵢₒ	FD8	DEMON
D8	—				
Rho8	1	—			
Dᵢₒ	3	0	—		
FD8	3	2	3	—	
DEMON	3	1	1	2	—

(b) Low elevation landscape classes

	D8	Rho8	Dᵢₒ	FD8	DEMON
D8	—				
Rho8	0	—			
Dᵢₒ	0	0	—		
FD8	0	1	0	—	
DEMON	1	1	0	1	—

(c) All landscape classes

	D8	Rho8	Dᵢₒ	FD8	DEMON
D8	—				
Rho8	1	—			
Dᵢₒ	3	0	—		
FD8	3	3	3	—	
DEMON	4	2	1	3	—

The counts for the three low elevation landscape classes summarized in Table IXb point to a very different story. The null hypothesis was never rejected for Dᵢₒ and rejected on only one of four occasions for D8. Rho8, FD8, and DEMON produced the largest differences—Rho8 and FD8 performed like the other flow algorithms in two of four cases and DEMON performed like the other four algorithms in only one of four instances.

The counts across all six landscape classes summarized in Table IXc show that Rho8 and Dᵢₒ were most like each other—the null hypothesis was never rejected for this pair of algorithms—followed by the D8/Rho8 and Dᵢₒ/DEMON pairs—the null hypothesis that the mean difference was not significantly different than zero was rejected for only one of six landscape classes in these instances. These counts also show that D8 and DEMON were least like each other, since the null hypothesis was rejected in four of six landscape classes for this pair of flow-routing algorithms.

The comparisons discussed thus far are good from the point of view that they show how often and where these different algorithms performed the same or not, but they fall short of indicating which algorithms make the most sense in terms of hydrologic theory and/or observation. A further look at the distribution of 'low flow' and 'channel' cells (using the same definitions used in Figures 5 and 6) across the six landscape classes provides some additional insights about the performance of the five flow-routing algorithms.

Table X highlights several noteworthy features about the distribution of low flow cells predicted with the five flow algorithms across the six landscape classes. First, the number of low flow cells predicted with the five flow-routing algorithms varied from 169 171 (Rho8) to 33 756 (DEMON). Second, the percentage of low flow cells in the hilltop/ridgeline class varied by a factor of five—from a low of 9% for DEMON to a high of 45% for D8 and, in general, these percentages indicate the presence of a series of broad hilltops and ridgelines in the study area. Third, Rho8 predicted >5000 low flow cells

Table X. Distribution of source cells (SCA ≤ 10 m^2 m^{-1}) by landscape class

Topo-climatic class	Number of cells	Percentage of cells with SCA ≤ 10 m^2m^{-1}				
		D8	Rho8	Dᵢₒ	FD8	DEMON
Hilltops/ridgelines	256 012	114,186 (44·6%)	79 789 (31·2%)	64 966 (25·4%)	39 215 (15·3%)	23 583 (9·2%)
Steep south-facing slopes	323 989	1686 (0·5%)	25 568 (7·9%)	481 (0·1%)	107 (0·0%)	91 (0·0%)
Steep north-facing slopes	231 180	5630 (2·4%)	18 584 (8·0%)	331 (0·1%)	72 (0·0%)	86 (0·0%)
Moderately steep lower valley slopes	169 173	37 (0·0%)	8245 (4·9%)	175 (0·1%)	15 (0·0%)	9 (0·0%)
Coastal plains/gentle slopes	177 787	39 893 (22·4%)	36 526 (20·5%)	28 995 (16·3%)	16 709 (9·4%)	9960 (5·6%)
Stream channels	103 888	35 (0·0%)	459 (0·4%)	94 (0·1%)	62 (0·1%)	27 (0·0%)
Total area	1 262 029	161 467 (12·8%)	169 171 (13·4%)	95 042 (7·5%)	56 180 (4·5%)	33 756 (2·7%)

Table XI. Distribution of 'stream channel' cells (SCA $\geq$ 5300 m^2 m^{-1}) by landscape class

Landscape class	Number of cells	Percentage of cells with SCA $\geq$ 5300 m^2 m^{-1}				
		D8	Rho8	D∞	FD8	DEMON
Hilltops/ridgelines	256 012	0 (0·0%)	13 (0·0%)	15 (0·0%)	0 (0·0%)	1 (0·0%)
Steep south-facing slopes	323 989	8 (0·0%)	158 (0·0%)	133 (0·0%)	11 (0·0%)	5 (0·0%)
Steep north-facing slopes	231 180	5 (0·0%)	137 (0·1%)	159 (0·1%)	6 (0·0%)	6 (0·0%)
Moderately steep lower valley slopes	169 173	949 (0·6%)	1439 (0·9%)	1669 (1·0%)	1013 (0·6%)	810 (0·5%)
Coastal plains/gentle slopes	177 787	801 (0·5%)	1221 (0·7%)	1494 (0·8%)	884 (0·5%)	793 (0·4%)
Stream channels	103 888	26 866 (27·6%)	25 744 (24·8%)	27 853 (26·8%)	27 896 (26·9%)	25 678 (24·7%)
Total area	1 262 029	28 685 (2·3%)	28 766 (2·3%)	31 340 (2·5%)	29 885 (2·4%)	27 316 (2·2%)
Percentage of 'stream channel' cells in stream channel class	N/A	93·7	89·5	88·9	93·3	94·0

in five of the six landscapes and D8 predicted >5000 low flow cells for steep north-facing slopes—neither result is realistic. Overall, these results suggest that the D∞, FD8, and DEMON performed better than D8 and especially Rho8—the latter algorithm, in particular, has large numbers of low flow cells scattered across most of the fuzzy *k*-means landscape classes.

Table XI summarizes the number of channel cells predicted with the five flow-routing algorithms for each of the six landscape classes. The number of predicted channel cells varied from 27 316 (DEMON) to 31 340 (D∞), a difference of 13%. The six landscapes classes can be divided into three groups—the three higher elevation classes, the two middle classes, and the stream channel class—to facilitate closer examination of flow-routing algorithm performance in this instance. This approach suggests that DEMON performed best (given the low number of channel cells in the three higher elevation classes and highest percentage (94%) of channel cells in the final stream channel class), with the D8 and FD8 algorithms close behind. This last result was expected because (1) the D8 algorithm was used to calculate the topographic wetness index and sediment transport capacity index inputs in the landscape classification (more on this aspect later) and (2) the last pair of algorithms (D8 and FD8) should behave the same in these landscape classes because the specification of a maximum cross-grading area in TAPES-G meant that the FD8 algorithm reverted to D8 when this upslope contributing area threshold was exceeded. Rho8 and D∞ performed the worst given the 1000+ channel cells predicted in the middle two landscape classes and 100+ channel cells predicted in the three higher elevation landscape classes, which is clearly not very plausible.

DISCUSSION AND CONCLUSIONS

The research reported here aimed to (1) calculate the SCA with five different flow-routing algorithms; (2) divide the study area into a series of repeatable landscape units; and (3) compare and contrast the performance of the five flow-routing algorithms across these newly developed landscape units. Several tables and maps of two areas—one along the coast and one of an inland area—were utilized to identify and analyze the variation in SCA across the study area and in each of the six landscape classes. The results were presented in three parts and this same sequence is used below to discuss the wider significance of this work.

The first part described the variability of SCA across the whole study area. There are substantial differences (Table I). Two sets of DEM pixels were identified—low flow cells (SCA $\leq$ 10 m^2 m^{-1}) near hilltops and ridgelines and cells crossed by stream channels (SCA $\geq$ 5300 m^2 m^{-1})—and used to examine the similarities and differences in the performance of the flow-routing algorithms more closely. The two single-flow-direction algorithms (D8 and Rho8) generated greater proportions of low flow cells compared with the three multiple-flow direction algorithms (Table X). There was much less variation between the five algorithms in terms of the numbers of pixels classified as stream channel cells: D8 predicted the largest numbers of stream channel cells but FD8, D∞, Rho8, and DEMON followed closely behind (Table XI). The similar results predicted with D8 and FD8 were to be expected in this study because the version of FD8 implemented in TAPES-G switches to D8 when a user-specified maximum cross-grading (i.e. SCA) threshold is exceeded.

The second part described the division of the study area into six landscape classes. The results indicated that the fuzzy *k*-means procedure worked well (Tables IV and V show six distinct classes and the maps reproduced in Figures 8 and 9 show that the maximum membership values produced distinct spatial patterns). This method is attractive because all eight topo-climatic attributes used as inputs can be calculated from DEMs and it is repeatable—meaning that someone starting with the

DOI: 10.1002/hyp

same attributes and applying the same classification algorithm to the same study area is likely to produce the same classification. Burrough *et al.* (2001) produced a similar classification with coarser resolution DEMs for the Greater Yellowstone Area and demonstrated that the resulting classification had important consequences for the land cover present in that region. The landscape classes were used to examine the similarities and differences in the spatial patterns of the SCA estimated with the five flow-routing algorithms in the current study.

The inclusion of topographic wetness and sediment transport capacity indices in this classification meant that one flow-routing algorithm (D8) was used to perform the classification and then used to evaluate the performance of this same and four other flow-routing algorithms. This is a potentially circular approach, especially since some of our other work has shown that the number and character of final landscape classes is dependent on the number of input variables, choice of weights, distance measure, etc. used in the fuzzy classification (Deng and Wilson, 2006). To address this issue, we prepared four additional eight-class landscape classifications—one for each of the other four flow-routing algorithms—and used the Kappa statistic to evaluate the level of similarity between pairs of landscape class maps (Table XII). These results showed that the Rho8 landscape class maps were very different than the other four (Kappa coefficient $\leq$ 0·30 in all four instances) but that the D8, D∞, FD8, and DEMON derived landscape class maps agreed with one another more often than not (Kappa coefficient >0·50 in all six pair-wise comparisons). Further work is needed to document (1) the sensitivity of landscape classifications to the choice of flow-routing algorithm and (2) whether the results presented here are likely to persist across landscape classifications generated with the same input variables but different flow-routing algorithms.

Two features of the results that were generated when the SCA was tabulated and compared by landscape class in this particular study warrant closer scrutiny. The first concerned the null hypotheses—whether the flow-routing algorithms perform the same or differently in different parts of the landscape. The flow-routing algorithms produced the largest variations at high elevations but, as elevation decreased, the flow-routing algorithms behaved more like each other (Table VIII). None of the previous studies comparing the performance of flow-routing algorithms has identified these systematic variations.

Table XII. Kappa coefficients showing level of agreement for pairs of landscape classifications generated with same topographic attributes but different flow-routing algorithms

	D8	Rho8	D∞	FD8	DEMON
D8	—				
Rho8	0·30	—			
D∞	0·64	0·30	—		
FD8	0·61	0·29	0·68	—	
DEMON	0·52	0·26	0·56	0·78	—

We can also see whether the matched pairs *t*-test results can be used to classify the five flow-routing algorithms into three groups based on the number of downslope cells to which flow can be allocated. This is of interest because Desmet and Govers (1996) and Endreny and Woods (2003) grouped the flow-routing algorithms in terms of the level of dispersion that was possible: following their advice, D8 and Rho8 should have emerged as a pair since both algorithms direct all flow to one downslope neighbor, DEMON and D∞ should have performed similarly because both algorithms distribute flow to one or two downslope neighbors, and FD8 should have generated unique results because it directs flow to as many as eight downslope cells.

The results were mixed. The null hypothesis was rejected in one of six landscape classes for the *t*-tests comparing Rho8 and D8 (as would be expected), and three of six and two of six times for Rho8 and FD8 and Rho8 and DEMON, respectively. These results coupled with the fact that the null hypothesis was never rejected for Rho8 and D∞ (this pair of algorithms was more like each other than D8 and Rho8) would seem to contradict the results reported in this other pair of studies. In contrast, the null hypothesis could not be rejected for five of six landscape classes when comparing DEMON and D∞, and this result supports some of the findings of earlier studies. The null hypothesis was rejected 12 out of 24 times for tests involving FD8 across the six landscape classes (Table VIII). At higher elevations, the null hypothesis was rejected 10 of 12 times as compared to only 2 of 10 times at lower elevations. The null hypothesis was rejected 3 of 12 times for tests involving DEMON at lower elevations indicating that this algorithm produced the most unique results in these areas. Overall, the *t*-test results confirmed that the FD8 algorithm is the most unique algorithm among the five flow-routing algorithms but it was not clear how to rank the remainder of the algorithms examined in this study.

The second feature of the *t*-test results that warrants closer scrutiny involves the 'low flow' cells and cells crossed by channels because these should have occurred in specific landscape classes. The distribution of these cells provides additional insights about the plausibility of the SCA estimates. Most of the low flow cells should occur in hilltop/ridgeline areas (class 6) and occasionally along the margins of coastal plains (class 1). D8 and Rho8 scattered the low flow cells throughout the six landscape classes, whereas the vast majority (>99%) of the low flow cells predicted with D∞, DEMON, and FD8 were confined to the hilltop/ridgeline landscape class (Table X). Similarly, the channel cells should have been predicted in the stream channel landscape class, and all five flow-routing algorithms did quite well in this respect (Table XI). Indeed, the five flow-routing algorithms behaved more like each other as flow descended down the hillslopes given the fact that the number of times the null hypothesis was rejected at the 5% level of significance decreased going from the high (i.e. hilltops

DOI: 10.1002/hyp

and ridgelines) to the low elevation parts of the landscape (i.e. stream channels and coastal plains).

The effective management of the flooding, erosion, water quality, and/or water supply problems that characterize many regions of the world depends on our knowledge of the behavior of stream channel networks and their contributing areas (Moore *et al.*, 1993). Endreny and Woods (2003) summarized the scale issues and some of the other problems that are encountered using DEM-based flow-routing algorithms to predict flow paths and SCAs. Their results (and similar results from several other studies) suggest using one of the flow-routing algorithms that disperse flow to one or two or three neighboring cells. The results from this study partially support these findings—Rho8 and to a lesser extent the D8 single flow-routing algorithm produced too many low flow cells in the wrong parts of the landscape to support their adoption and use in these types of applications. Rho8 suffered the most in this respect and also produces unique outcomes each time it is used and, as a consequence, it should be avoided altogether. However, the D8 results are perhaps more troubling given the widespread adoption and use of this particular flow-routing algorithm in current geographic information systems. The results comparing Dοο, DEMON, and FD8 were less clear and indicate that further work incorporating field observations of runoff generation is required to determine whether one or more of these algorithms should be preferred in specific types of landscapes and/or applications.

ACKNOWLEDGEMENTS

We would like to thank two anonymous reviewers for their comments on an earlier version of this paper.

REFERENCES

Band L, Tague C, Brun S, Tenenbaum D, Fernandez R. 2000. Modelling watersheds as spatial object hierarchies: structure and dynamics. *Transactions in GIS* **4**: 181–196.

Barling RD, Moore ID, Grayson RD. 1994. A quasi-dynamic wetness index for characterizing the spatial distribution of zones and surface saturation and soil water content. *Water Resources Research* **30**: 1029–1044.

Beasley DG, Huggins LF, Monke EJ. 1980. ANSWERS: a model for watershed planning. *Transactions of the American Society of Agricultural Engineers* **23**: 938–946.

Beven KJ, Kirkby MJ. 1979. A physically based, variable contributing area model of basin hydrology. *Hydrological Sciences Bulletin* **24**: 43–69.

Burrough PA, McDonnell RA. 1998. *Principles of Geographical Information Systems*. Oxford University Press: New York.

Burrough PA, Wilson JP, van Gaans PFM, Hansen AJ. 2001. Fuzzy k-means classification of digital elevation models as an aid to forest mapping in the Greater Yellowstone area, USA. *Landscape Ecology* **16**: 523–546.

Costa-Cabral MC, Burges SJ. 1994. Digital elevation model networks (DEMON): a model of flow over hillslopes for computation of contributing and dispersal areas. *Water Resources Research* **30**: 1681–1692.

Deng YX, Wilson JP. 2006. Role of attribute selection in GIS representations of the biophysical environment. *Annals of the Association of American Geographers* **96**: 47–63.

Desmet PJJ, Govers G. 1996. Comparison of routing algorithms for digital elevation models and their implications for predicting ephemeral gullies. *International Journal of Geographical Information Systems* **10**: 311–331.

Dikau R. 1989. The application of a digital relief model to landform analysis. In *Three-dimensional Applications in Geographical Information Systems*, Raper JF (ed.). Taylor and Francis: London; 51–77.

Eastman JR. 1992. *IDRISI (Version 4.0): Geographic Information System Software and Documentation*. Graduate School of Geography, Clark University: Worcester, MA.

Endreny TA, Woods EW. 2003. Maximizing spatial congruence of observed and DEM-delineated overland flow networks. *International Journal of Geographical Information Science* **17**: 699–713.

Fairfield J, Leymarie P. 1991. Drainage networks from grid digital elevation models. *Water Resources Research* **27**: 709–717.

Freeman GT. 1991. Calculating catchment area with divergent flow based on a regular grid. *Computers & Geosciences* **17**: 413–422.

Fried JS, Brown DG, Zweifler MO, Gold MA. 2000. Mapping contributing areas for stormwater discharge to streams using terrain analysis. In *Terrain Analysis: Principles and Applications*, Wilson JP, Gallant JC (eds). John Wiley and Sons: New York; 183–203.

Gallant JC, Wilson JP. 1996. TAPES-G: a grid-based terrain analysis program for the environmental sciences. *Computers & Geosciences* **22**: 713–722.

Gallant JC, Wilson JP. 2000. Primary topographic attributes. In *Terrain Analysis: Principles and Applications*, Wilson JP, Gallant JC (eds). John Wiley and Sons: New York; 51–85.

Gallant JC, Hutchinson MF, Wilson JP. 2000. Future directions for terrain analysis. In *Terrain Analysis: Principles and Applications*, Wilson JP, Gallant JC (eds). John Wiley and Sons: New York; 423–427.

Garbrecht J, Martz LW. 1997. The assignment of drainage directions over flat areas in raster Digital Elevation Models. *Journal of Hydrology* **193**: 204–213.

Huffman M. 1998. *Wild Heart of Los Angeles: The Santa Monica Mountains*. Roberts Rinehart Publishers: Niwot, CO.

Hutchinson MF. 1989. A new procedure for gridding elevation and stream line data with automatic removal of pits. *Journal of Hydrology* **106**: 211–232.

Jensen JR. 1996. *Introductory Image Processing: A Remote Sensing Perspective*, 2nd edn. Prentice-Hall: Upper Saddle Creek, NJ.

Karssenberg D, Burrough PA, Sluiter R, de Jong K. 2001. The PCRaster software and course materials for teaching numerical modeling in the environmental sciences. *Transactions in GIS* **5**: 99–110.

Lea NL. 1992. An aspect driven kinematic routing algorithm. In *Overland Flow: Hydraulics and Erosion Mechanics*, Parsons AJ, Abrahams AD (eds). University College London Press: London; 393–407.

Mitasova H, Mitas L. 2002. Modeling physical systems. In *Geographic Information Systems and Environmental Modeling*, Clarke KC, Parks BO, Crane MP (eds). Prentice-Hall: Upper Saddle River, NJ; 189–210.

Moore ID. 1996. Hydrologic modeling and GIS. In *GIS and Environmental Modeling: Progress and Research Issues*, Goodchild MF, Steyaert LT, Parks BO, Johnston C, Maidment D, Crane M, Glendinning S (eds). GIS World Books: Fort Collins, CO; 143–148.

Moore ID, Hutchinson MF. 1991. Spatial extension of hydrologic process modeling. *Proceedings of the International Hydrology and Water Resources Symposium*. Institute of Australian Engineers: Perth, Canberra; 803–808, 2–4 October.

Moore ID, Wilson JP. 1992. Length-slope factors for the revised universal soil loss equation: a simplified method of estimation. *Journal of Soil and Water Conservation* **47**: 423–428.

Moore ID, Wilson JP. 1994. Reply to comments by Foster on "length-slope factors for the revised universal soil loss equation: a simplified method of estimation". *Journal of Soil and Water Conservation* **49**: 174–180.

Moore ID, Burch GJ, MacKenzie DH. 1988. Topographic effects on the distribution of surface soil water and the location of ephemeral gullies. *Transactions of the American Society of Agricultural Engineers* **31**: 1098–1107.

Moore ID, Grayson RB, Ladson AR. 1991. Digital terrain modeling: a review of hydrological, geomorphological, and biological applications. *Hydrological Processes* **5**: 3–30.

Moore ID, Turner AK, Wilson JP, Jenson SK, Band LE. 1993. GIS and land surface-subsurface modeling. In *Environmental Modeling with GIS*, Goodchild MF, Parks BO, Steyaert LT (eds). Oxford University Press: New York; 196–230.

O'Callaghan JF, Mark DM. 1984. The extraction of drainage networks from digital elevation data. *Computer Vision Graphics and Image Processing* **28**: 328–344.

Peters DL, Buttle JM, Taylor CH, LaZerte BD. 1995. Runoff production in a forested, shallow soil, Canadian Shield basin. *Water Resources Research* **31**: 1291–1305.

Quinn PF, Beven KJ, Chevallier P, Planchon O. 1991. The prediction of hillslope flow paths for distributed hydrological modeling using digital terrain models. *Hydrological Processes* **5**: 59–79.

Sulebak JR, Tallaksen LM, Erichsen B. 2000. Estimation of areal soil moisture by use of terrain data. *Geografiska Annaler Series A-Physical Geography* **82**: 89–105.

Tarboton DG. 1997. A new method for the determination of flow directions and upslope areas in grid digital elevation models. *Water Resources Research* **33**: 309–319.

Wilson JP, Gallant JC. 2000. Digital terrain analysis. In *Terrain Analysis: Principles and Applications*, Wilson JP, Gallant JC (eds). John Wiley and Sons: New York; 1–27.

Wilson JP, Repetto RL, Snyder RD. 2000. Effect of data source, grid resolution, and flow-routing method on computed topographic attributes. In *Terrain Analysis: Principles and Applications*, Wilson JP, Gallant JC (eds). John Wiley and Sons: New York; 133–161.

Wolock DM, McCabe GJ. 1995. Comparison of single and multiple flow direction algorithms for computing topographic parameters in TOPMODEL. *Water Resources Research* **31**: 1315–1324.